18

^{13}C-Metabolic Flux Analysis and Metabolic Regulation

Yu Matsuoka[1] and Kazuyuki Shimizu[1,2]
[1]*Depatment of Bioscience and Bioinformatics, Kyushu Institute of Technology*
[2]*Institute of Advanced Bioscience, Keio University*
Japan

1. Introduction

Among the different levels of information in a cell, the most important information in understanding the complex metabolic control mechanism of the whole cell may be the metabolic flux distribution in the central metabolism (Sauer, 2006), as this is the manifestation of gene and protein expressions and the concentrations of intracellular metabolites (Matsuoka & Shimizu, 2010a) (Fig.1), where a set of metabolic fluxes (or enzyme activities) describes the cell physiology (Bailey, 1981). The information of the metabolic flux distribution is quite useful for metabolic engineering (Stephanopoulos, 1999).

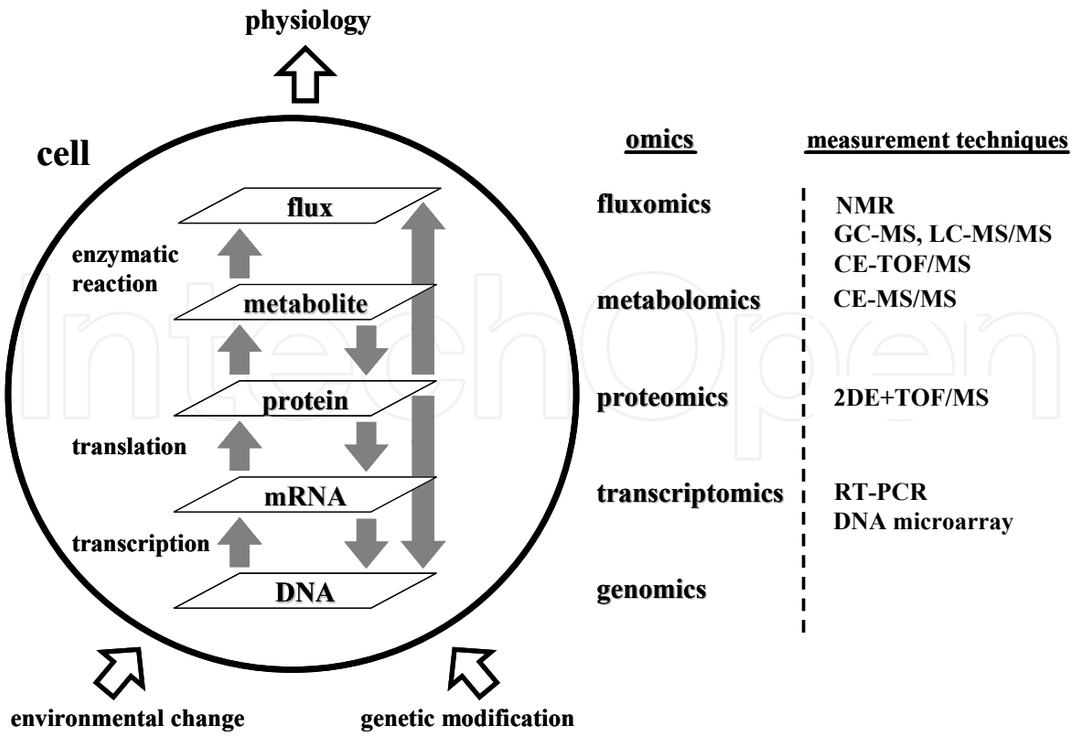

Fig. 1. Illustration of different levels of information in the cell.

In principle, metabolic flux analysis is based on mass conservation of key metabolites. The intracellular fluxes can be calculated from the measured specific rates by applying mass balances to these intracellular metabolites (Stephanopoulos et al., 1998) together with stoichiometric equations. The number of measureable extracellular fluxes is limited in practice, and the stoichiometric constraints often lead to an underdetermined algebraic system. Therefore, cofactor balances are sometimes required to be introduced into the stoichiometric model, or appropriate objective functions has to be introduced for optimization to determine the fluxes. The central metabolic pathway has both anabolic and catabolic functions, as it provides cofactors and building blocks for macromolecular system (anabolism) as well as energy (ATP) production (catabolism). The optimization may be made in terms of catabolism and anabolism, or both, under the constraints of the stoichiometric equations. Flux balance analysis (FBA) has been extensively used to predict the steady-state metabolic fluxes in order to maximize the cell growth rate (Edwards & Palsson, 2000; Schilling & Palsson, 1998; Price et al., 2003). However, the accuracy of the flux calculation depends on the validity of the cofactor assumptions and an appropriate choice of the objective function(s) employed (Schuetz et al., 2007). The presence of unknown reactions that generate or consume the cofactors may invalidate the assumption that their concentrations remain in balance, and the selected objective functions may not be appropriate, or their validity may be limited to certain states of the cell. Namely, this approach cannot essentially compute such fluxes as (1) recycled fluxes, (2) bidirectional fluxes, and (3) parallel fluxes due to the singularity of the stoichiometric matrix. Note, however, that the conventional FBA may be reasonably applied for the case without recycles such as anaerobic or micro-aerobic cultivation (Zhu & Shimizu, 2004, 2005). ^{13}C-Metabolic flux analysis has been developed to overcome such problems as stated above and to estimate *in vivo* fluxes in more accurately. In this chapter, ^{13}C-metabolic flux analysis (^{13}C-MFA) is explained with some appications. The analytical approach for ^{13}C-MFA is given to understand the feature of this method, and the basic principle of isotopomer dynamics is also explained. Finally, the metabolic regulation mechanism is also mentioned in view of global regulators.

2. ^{13}C-Metabolic flux analysis (^{13}C-MFA) and its application

For ^{13}C-metabolic flux analysis, isotopically labeled substrates are introduced to the cell, and the labeled carbon atoms are distributed throughout its metabolic network. The final isotopic enrichment in the intracellular metabolite pools can then be measured (Matsuoka & Shimizu, 2010a) (Fig. 2). The amino acids in biomass hydrolysate are much more abundant than their precursors in the cell metabolism, and it has been often used to deduce the labeling patterns of the intracellular metabolites from that of the proteinogenic amino acids, based on precursor-amino acids relationships (Szyperski, 1995). Either NMR spectroscopy or GC-MS has been extensively used for the isotopic tracer experiments. NMR is used to measure the positional ^{13}C enrichment (Szyperski, 1995; Marx et al., 1996). Although ^{13}C NMR is powerful and attractive for metabolic flux analysis, it requires relatively large amount of sample. On the other hand, GC-MS can easily analyze metabolites with much less amount of sample. As a result, it may be suitable for flux analysis of the culture processes that have low concentrations of biomass (Fischer & Sauer, 2003; Wittmann, 2007). Currently, these tracer techniques, in combination with direct extracellular flux measurements, are considered to be a powerful method for obtaining intracellular metabolic flux distribution (MFD) using only a few modeling assumptions (Stephanopoulos, 1999; Marx et al., 1996;

Schmidt et al., 1999; Wiechert & Graaf, 1997; Sauer, 2004). Alternatively, flux ratio analysis can be used to constrain the fluxes at the important branch point (Szyperski et al., 1999; Fischer & Sauer, 2003; Sauer et al., 1999; Hua et al., 2003).

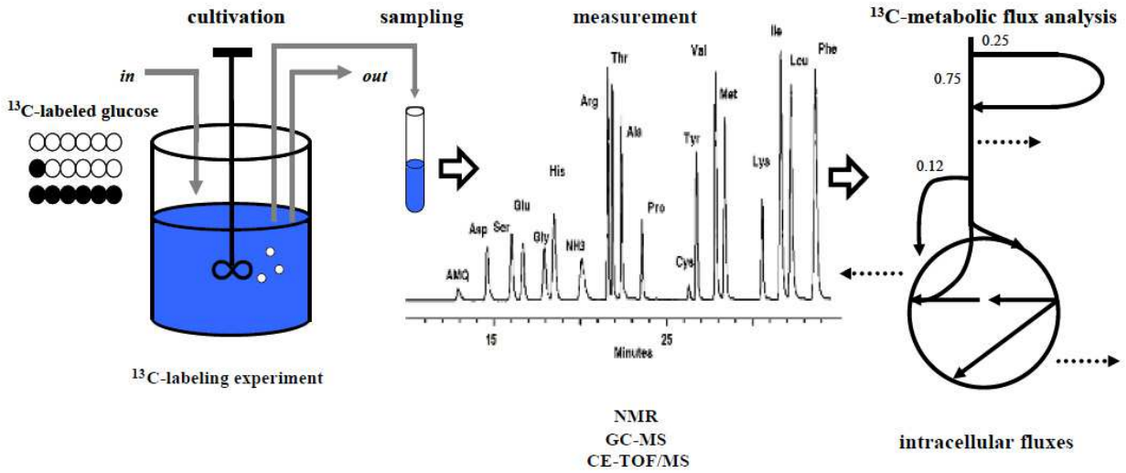

Fig. 2. ^{13}C-Metabolic flux analysis by ^{13}C-labeling experiment, the measurement of isotopomer distribution, and the flux determination.

^{13}C-Metaolic flux analysis has been applied to such microorganisms as *Escherichia coli*, *Corynebacterium glutamicum*, *Saccharomyces cerevisiae* (Blank & Sauer, 2004; Raghevendran et al., 2004), *Bacillus subtilis* (Sauer et al., 1997), acetic acid bacterium *Gluconacetobacter oboediens* (Sarkar et al., 2010), and others (Fuhrer et al., 2005), and its application has been extended to other organisms such as Cyanobacteria (Yang et al., 2002a, b), plant cells (Schwender et al., 2004), and mammarian cells (Sherry et al., 2004; Kelleher, 2004; Hellerstein, 2004; Sidorenko et al., 2008), including mouse (McCabe & Previs, 2004), brain (Rothman et al., 2003), neural cells (Selivanov et al., 2006), and cancer cells (Selivanov et al., 2005) and so on.

Let us consider the several single-gene knockout mutants such as *zwf, gnd* and *pgi* gene knockout. Figure 3 shows how the NMR spectra patterns change for *pgi* gene knockout mutant as compared to wild type, where it shows the relative intensities of ^{13}C-^{13}C scalar coupling multiplet spectra patterns of amino acid measured by NMR, where the samples were taken from the labeling experiments using a mixture of [U-^{13}C] and unlabeled [U-^{12}C] glucose conducted under aerobic steady state condition (Hua et al., 2003). The differences between NMR spectra patterns of wild type and *pgi* gene knockout mutant result in different flux distribution. Based on NMR data such as shown in Fig. 3, Fig. 4 shows the result of ^{13}C-metabolic flux analysis for wild type and *pgi* gene knockout mutant cultivated in the continuous culture at the dilution rate of 0.1 h^{-1} (Hua et al., 2003). It can be seen that the knockout of *pgi* gene, which codes for the first enzyme of the EMP (Embden-Meyerhoff-Parnas) pathway after the branch point at G6P, resulted in exclusive use of the oxidative pentose phosphate (PP) pathway for glucose catabolism. The overproduced NADPH inhibits the activity of G6PDH thus reduces the glucose consumption rate, resulting in the low growth rate. The glyoxylate pathway was activated, and the Entner-Doudoroff (ED) pathway was activated in this mutant. The activation of ED pathway may be due to reducing NADPH production as compared to employing 6PGDH pathway. The activation of the glyoxylate pathway is considered to be due to the feedback regulation to compensate for the lowered

OAA concentration caused by the lowered flux of EMP pathway and the lowered anaplerotic flux through Ppc to supply OAA.

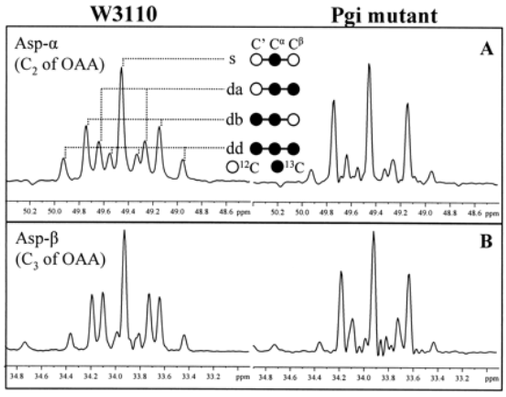

Fig. 3. ^{13}C-^{13}C scalar coupling multiplets observed for aspartate from glucose-limited chemostat cultures of *E. coli* W3110 (left) and the *pgi* mutant (right). The signals were extracted from the $\omega_1(^{13}C)$ cross sections in the [^{13}C,^{1}H]-COSY spectra. (A) Asp-α; (B) Asp-β. As indicated in panel A, the multiplets consist of a singlet (s), a doublet with a small coupling constant (da), a doublet split by a larger coupling constant (db), and a doublet of doublets (dd). Aspartate corresponds directly to its metabolic precursor, OAA.

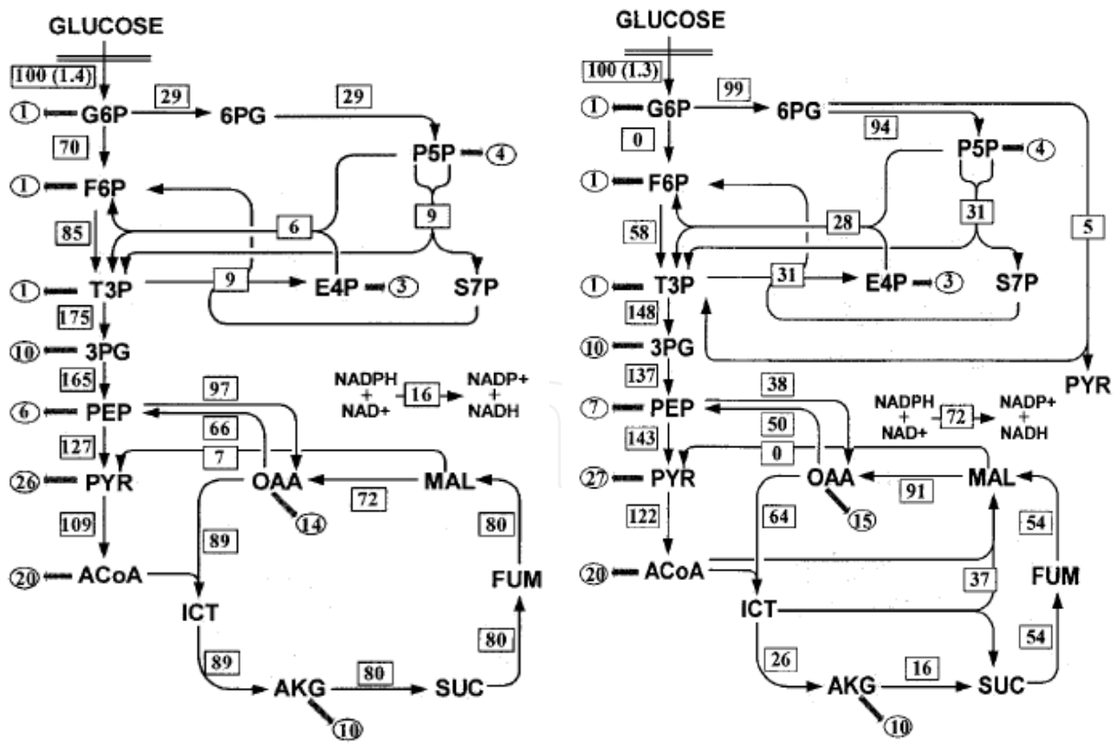

Fig. 4. Metabolic flux distributions of (a) *E. coli* wild type and (b) its *pgi* gene knockout mutant under glucose-limited continuous cultivation at the dilution rate of 0.1 h^{-1}.

Let us consider next the *zwf* or *gnd* gene knockout mutants, where the ^{13}C-metabolic flux distributions are given in Fig. 5 in the cases of using glucose (Fig. 5a) and pyruvate (Fig. 5b) (Zhao et al., 2004). Since the flux through oxidative PP pathway was significantly decreased or totally blocked in the mutants grown on glucose, the metabolic network has to give a higher flux through EMP or ED pathway to the TCA cycle. The opposite relations are seen in mutants grown on pyruvate, where the deletion of genes caused a reduction in the fluxes through the TCA cycle.

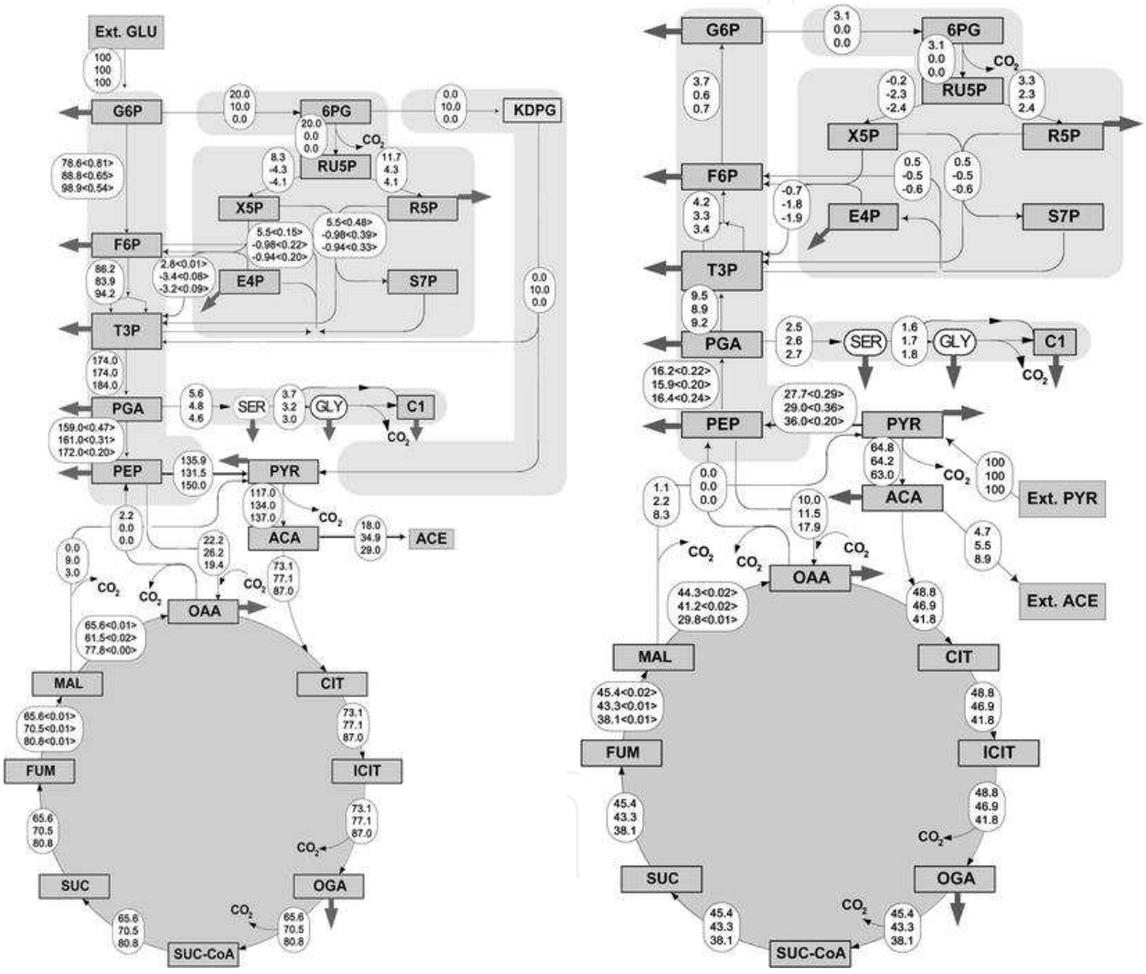

Fig. 5. Metabolic flux distributions in chemostat culture of (a) glucose-grown and (b) pyruvate-grown *E. coli* parent strain (*upper values*), *gnd* (*middle values*), and *zwf* (*lower values*) mutants at D=0.2 h^{-1}.The exchange coefficients are shown in brackets for the reactions that were considered reversible. *Negative values* indicate the reversed pathway direction.

3. Analytical approach to ^{13}C-metabolic flux analysis

Let us consider how the fluxes are computed based on ^{13}C-labeled metabolites. For this, consider how the isotopomer pattern changes with respect to fluxes. Let us cosider TCA cycle for the case of using pyruvate or acetate as a carbon source, where fate of carbons is shown in Fig. 6 (Matsuoka & Shimizu, 2010b).

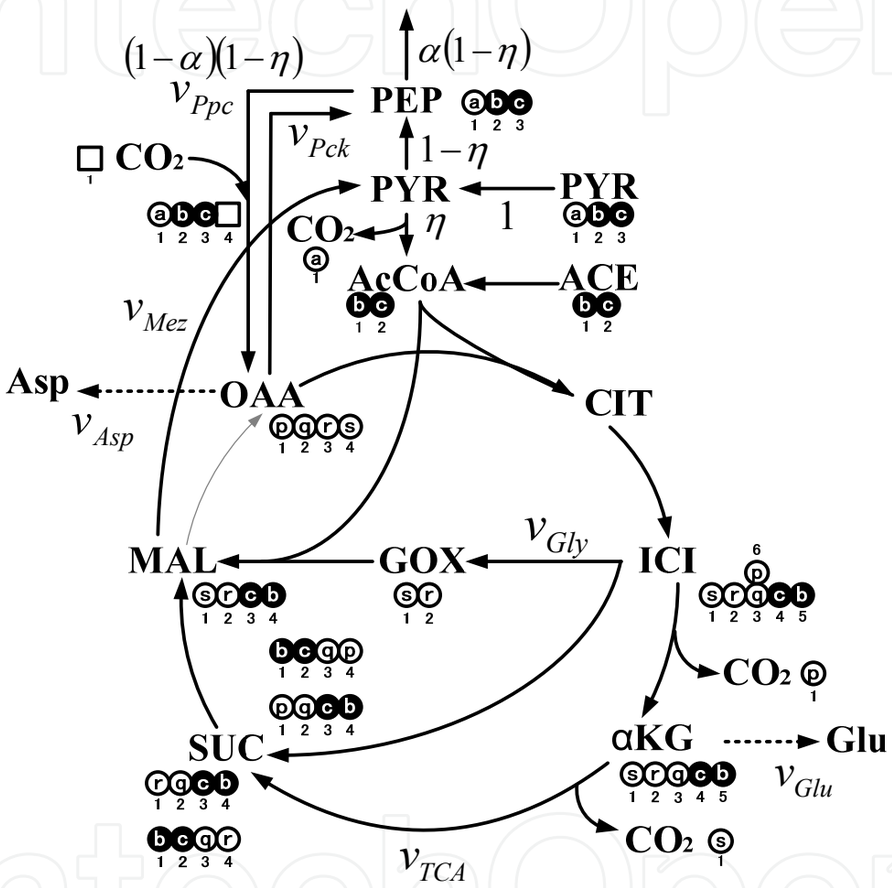

Fig. 6. Metabolic network for the change in isotopomer distribution: pyruvate or acetate as a carbon source.

Referring to Fig. 6, let η be the flux toward AcCoA from PYR, and let $(1-\eta)$ be the other flux toward PEP. Moreover, let α be the fraction toward gluconeogenic pathway from PEP, and let $(1-\alpha)$ be the other fraction toward anaplelotic pathway through Ppc to OAA. From the mass balance for OAA, the normalized molar formation rate of OAA is expressed as $v_{OAA}^{+} = v_{TCA} + 2v_{Gly} - v_{Mez} + v_{Ppc}$, and the molar consumption rate of OAA is expressed as $v_{OAA}^{-} = v_{TCA} + v_{Gly} + v_{Glu} + v_{Asp} + v_{Pck}$. Since $v_{OAA}^{+} = v_{OAA}^{-}$ holds at steady state, the following expression can be derived:

$$v_{Gly} + v_{Ppc} = v_{Glu} + v_{Asp} + v_{Mez} + v_{Pck} \tag{1}$$

Since $v_{Ppc} = (1-\alpha)(1-\eta) + v_{Pck}$ holds, the following expression can be derived:

$$(1-\eta)\alpha = 1 - \eta + v_{Gly} - \left(v_{Glu} + v_{Asp} + v_{Mez}\right) \tag{2}$$

Then the isotopomer balance for O_1 may be expressed as

$$\begin{aligned} &\frac{1}{2}\left(1-\frac{w}{1+2z}\right)\left[\left(O_3 + O_{13} + O_{34} + O_{134}\right)A_0 + \left(O_0 + O_1 + O_4 + O_{14}\right)A_1\right] \\ &+\frac{z}{2}\left(1-\frac{w}{1+2z}\right)\left[\begin{array}{l} 2\left(O_0 + O_1 + O_2 + O_{12}\right)A_1 + \left(O_1 + O_{13} + O_{14} + O_{134}\right)A_0 + \\ \left(O_0 + O_3 + O_4 + O_{34}\right)A_1 \end{array}\right] \\ &+ yP_1C_0 = (1 + 2z - w + y)O_1 \end{aligned} \tag{3}$$

where, $w \equiv v_{Mez}/v_{TCA}$, $y \equiv v_{Ppc}/v_{TCA}$, and $z \equiv v_{Gly}/v_{TCA}$. Note that the LHS of Eq. (3) is the formation rate of O_1 , and the RHS is the consumption rate of O_1 . In Eq. (3), A_i and P_j are the mole fractions of acetate and PYR isotopomers labeled at i -th and j -th carbons, respectively, and C_k $(k = 0, 1)$ is the mole fraction of labeled CO_2 through Ppc reaction. The similar equations can be derived for all the other isotopomers, and the set of equations can be expressed as

$$\Lambda_{AP} I_{OAA} = b_{AP} \tag{4}$$

where Λ_{AP} $(\in R^{16} \times R^{16})$ is the coefficient matrix, and b_{AP} $(\in R^{16})$ is the residual vector, where the detailed matrix and vector are given elsewhere (Matsuoka & Shimizu, 2010b). Eq. (4) may be solved as

$$I_{OAA} = {\Lambda_{AP}}^{-1} b_{AP} \tag{5}$$

if Λ_{AP} is nonsingular. In this case, Eq. (4) cannot be solved directly. Recall that the isotopomer fractions must be summed up to 1, namely the following equation must be satisfied:

$$\sum_i O_i = 1 \tag{6}$$

Therefore, Eq. (4) can be solved by replacing one of the equations using Eq. (6).

Let us consider the special case where 100 % [1-^{13}C] pyruvate is used as a carbon source, and it is set $v_{Mez} = 0$ and $v_{Pck} = 0$ for simplicity. Then Eq. (5) gives the following equation (Matsuoka & Shimizu, 2010b):

$$\begin{bmatrix} O_0 \\ O_1 \\ O_4 \end{bmatrix} = \begin{bmatrix} \dfrac{1}{1+y} \\ \dfrac{y}{1+y} \\ 0 \end{bmatrix} \tag{7}$$

In the case where 100 % [2-^{13}C] pyruvate is used, the following equations can be derived (Matsuoka & Shimizu, 2010b):

$$O_1 = O_4 = \frac{1}{2(1+y)^2(1+2y)} \tag{8a}$$

$$O_2 = \frac{y}{1+y} \tag{8b}$$

$$O_{13} = O_{24} = \frac{y}{(1+y)(1+2y)} \tag{8c}$$

$$O_{14} = \frac{y}{(1+y)^2(1+2y)} \tag{8d}$$

In the case where 100 % [3-^{13}C] pyruvate is used, the following expressions can be derived (Matsuoka & Shimizu, 2010b):

$$O_2 = 0 \tag{9a}$$

$$O_3 = \frac{y}{1+y} \tag{9b}$$

$$O_{13} = O_{24} = \frac{y}{(1+y)(1+2y)} \tag{9c}$$

$$\begin{bmatrix} O_{23} \\ O_{123} \\ O_{234} \end{bmatrix} = \begin{bmatrix} \dfrac{y}{(1+y)^2(1+2y)} \\ \dfrac{1}{2(1+y)^2(1+2y)} \\ \dfrac{1}{2(1+y)^2(1+2y)} \end{bmatrix} \tag{9d}$$

Let us consider the case of using acetate as a carbon source by letting $v_{Ppc} = 0$ in Fig. 6. If the mixture of [1-^{13}C] acetate (A_1) and the unlabeled acetate is used, only 4 isotopomers (O_0, O_1, O_4, O_{14}) are present, and if $A_1 = 1$, those can be expressed as (Matsuoka & Shimizu, 2010b)

$$\begin{bmatrix} O_1 \\ O_4 \\ O_{14} \end{bmatrix} = \begin{bmatrix} \dfrac{1+2z}{(1+z)(2+3z)} \\ \dfrac{1}{2+3z} \\ \dfrac{z}{1+z} \end{bmatrix} \tag{10}$$

If [2-^{13}C] acetate (A_2) and the unlabeled acetate are used as a carbon source, 12 isotopomers are present, and those reduce to 3 isotopomers when $A_2 = 1$ as follows (Matsuoka & Shimizu, 2010b):

$$\begin{bmatrix} O_{23} \\ O_{123} \\ O_{234} \end{bmatrix} = \begin{bmatrix} \dfrac{z}{1+z} \\ \dfrac{1}{2+3z} \\ \dfrac{1+2z}{(1+z)(2+3z)} \end{bmatrix} \tag{11}$$

Figure 7 shows how the isotopomer distribution changes with respect to η for the case of using 100 % of [3-^{13}C] pyruvate as a carbon source (Matsuoka & Shimizu, 2010a). It indicates that OAA isotopomers as well as mass isotopomers change with respect to η in somewhat strange way, where Fig. 7c explains for the cases of $\eta = 0$ (left), $0 < \eta < 1$ (middle), and $\eta = 1$ (right). In Fig. 7a, O_3 increases as η becomes low. This is due to Ppc reaction (left figure in Fig. 7c). The case where η is low, most of the [3-^{13}C] pyruvate goes to OAA via Ppc and generates O_3 . As proceeding TCA cycle, O_3 and [2-^{13}C] AcCoA (originated from [3-^{13}C] PYR since the 1st carbon of PYR is lost as CO_2 at PDHc reaction) generate O_{13} and O_{24} by the 1st turn of the TCA cycle, where O_{24} further generates O_{23} in the 2nd turn, and in turn O_{23} generates O_{123} and O_{234} at the 3rd turn of the TCA cycle (middle figure in Fig. 7c). Thus O_3 , O_{13} , O_{24} , O_{23} , O_{123} , and O_{234} are eventually generated, where the amount of O_3 is the highest at low values of η , but the fractions of O_{13} and O_{24} become higher as TCA cycle flux increases. When η is high, where most flux goes through PDHc reaction, A_2 (P_3) generates O_2 and O_3 at the 1st turn of TCA cycle, and in turn O_2 and A_2 generate O_{23} , while O_3 and A_2 generate O_{13} and O_{24} in the 2nd turn. Moreover, O_{23} and A_2 generate O_{123} and O_{234} at the 3rd turn and so on. Namely, O_{123} and O_{234} become higher as cycling the TCA cycle, and thus those become higher at the steady state (right figure in Fig. 7c). The above observation implies that the fraction of O_3 becomes higher as η is low, whereas the fractions of O_{13} and O_{24} become higher as η increases, and then the fractions of O_{123} and O_{234} become higher as η becomes further higher. This is the reason why O_{13} , O_{24} , and O_{23} give maximum with respect to η as seen in Fig. 7a. Figure 7b shows how the mass isotopomers change with respect to η . It indicates that m_1 decreases while m_3 increases as η increases, whereas m_2 becomes maximum at certain value of η . This is due to the changing patterns of $O_{13} = O_{24}$ and O_{23} as seen in Fig. 7a. These illustrate the complexity of the ^{13}C-flux analysis in relation to TCA cycle. The transitions of the isotopomers with respect to turn of TCA cycle may be expressed in more systematic way by introducing the transition matrix.

Consider next the case of using glucose as a carbon source. Referring to Fig. 8 (Matsuoka & Shimizu, 2010a), let v_1 be the normalized flux toward glycolysis at glucose 6-phosphate (G6P) and let $1 - v_1$ be the flux toward oxidative pentose phosphate (PP) pathway, where the input flux to the system is normalized to be 1 without loss of generality. Then the mass balance equations can be derived for each metabolite. Moreover, isotopomer balances may be considered for each metabolite. Since glucose has 6 carbons, the number of its isotopomers is $2^6 = 64$ and let these be expressed as $G_0, G_1, \cdots, G_{123456}$, where G_0 denotes unlabeled glucose, G_1 denotes [1-^{13}C] glucose, and G_{123456} denotes [U-^{13}C] glucose and so on. The number of

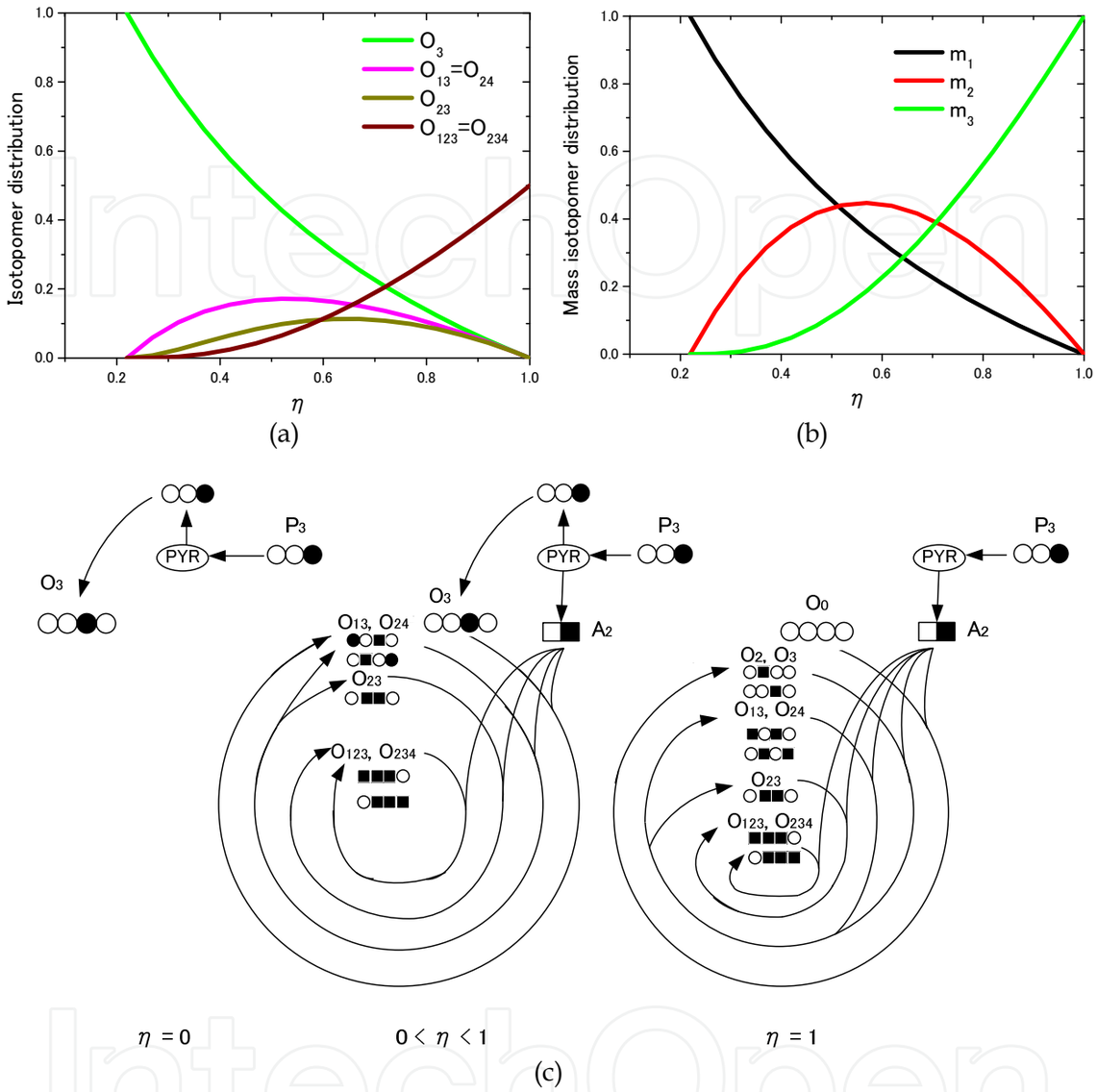

Fig. 7. Effect of η on (a) isotopomer and (b) mass isotopomer distributions for the case of using 100 % [3-^{13}C] pyruvate ($\alpha = 0.4$). (c) schematic illustration of how the specific isotopomers are generated.

isotopomer balance equations is $2^6 = 64$ for G6P, $2^5 = 32$ for P5P (Ru5P, X5P, R5P), $2^7 = 128$ for S7P, $2^4 = 16$ for E4P, $2^6 = 64$ for F6P, and $2^3 = 8$ for GAP. The same number of isotopomers is present, and therefore, the isotopomer distribution for each metabolite can be obtained uniquely as a function of the labeling patterns of glucose on condition that the fluxes are given. Consider the case of using 100 % of [1-^{13}C] glucose as a carbon source for simplicity. It may be easily shown that GAP_3 decreases, while GAP_0 increases as v_1 decreases, because the labeled 1st carbon is lost at 6PGDH reaction in the PP pathway, and thus the flux v_1 may be identified by the mass isotopomer patterns of GAP (or Ser).

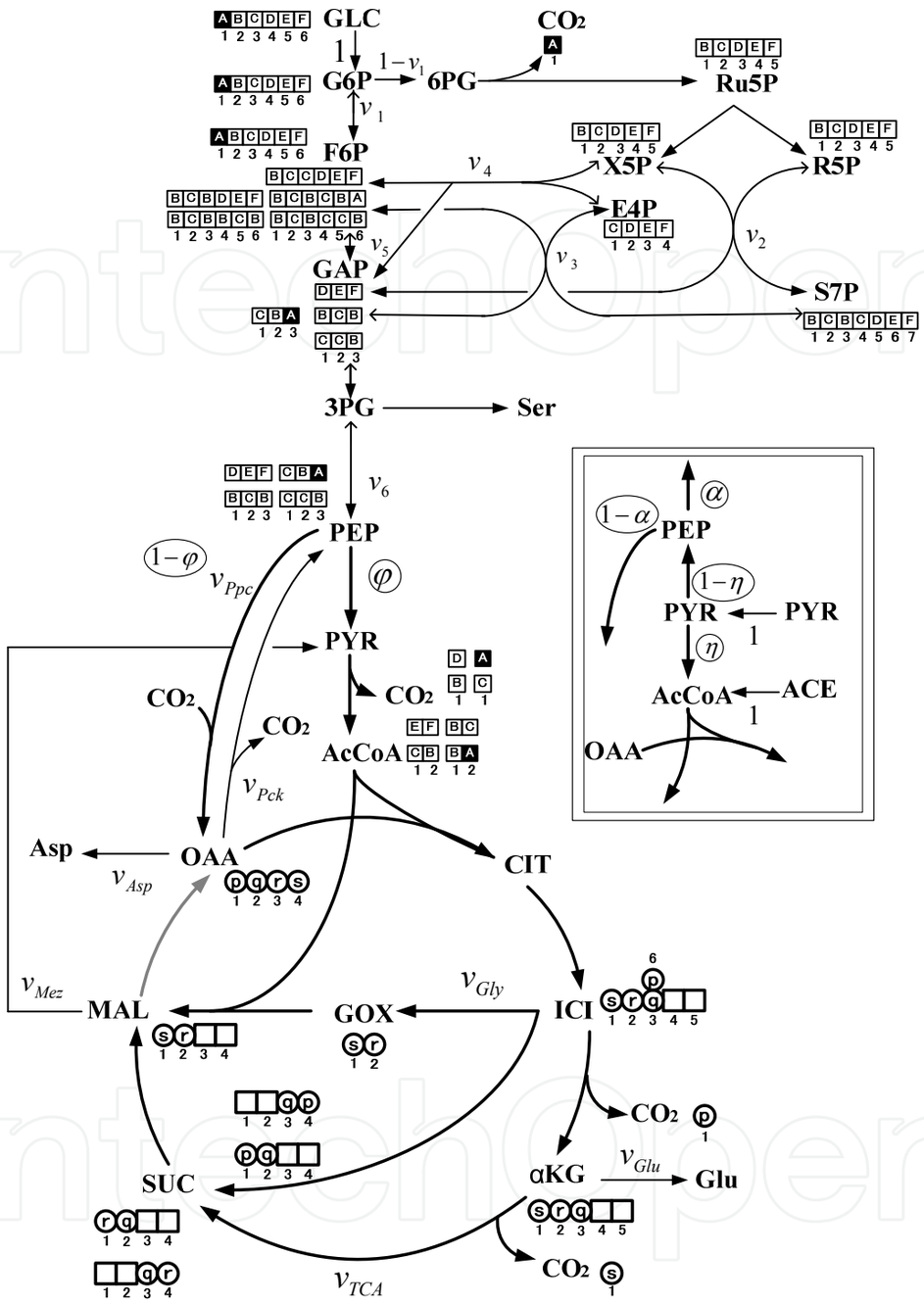

Fig. 8. Main metabolic pathways in the central metabolism together with the fate of [1-[13]C] glucose.

Consider next how the isotopomers of GAP affect those of TCA cycle. Referring to Fig. 8, Let ϕ be the fraction from PEP to PYR through Pyk, and let $1-\phi$ be the rest of the fraction which flows from PEP to OAA by the anaplerotic pathway. Figure 9a shows the effect of ϕ on the isotopomer distribution of OAA, and Fig. 9b shows its effect on the mass isotopomer distribution using 100 % of [1-[13]C] glucose for the case where $v_1 = 1$ for simplicity

(Matsuoka & Shimizu, 2010a). Note that O_i is the isotopomer of OAA labeled at i-th carbon(s) and m_j is the mass isotopomer, where it is the linear combination of the isotopomers of OAA. For example, $m_0 = O_0$, $m_1 = \sum_{i=1}^{4} O_i$, and so on. Unlike glycolysis and PP pathway, TCA cycle provides a variety of isotopomers as given in Fig. 9a, and Fig. 9b indicates that ϕ may be identified by MS measurement of $m_0 \sim m_3$. The reason why m_1 is less sensitive with respect to ϕ as compared to the other mass isotopomers is that O_2 increases while O_3 decreases as ϕ increases. Note that GAP_3 and GAP_0 are generated at Fba reaction from [1-^{13}C] glucose. Those bring O_3 and O_0 via Ppc reaction. Another isotopomers such as O_2 and O_{23} appear as proceeding TCA cycle (Matsuoka & Shimizu, 2010a). Although [1-^{13}C] glucose and/or [U-^{13}C] glucose are exclusively used in practice, [1, 2-^{13}C] glucose may be also used for the flux estimation.

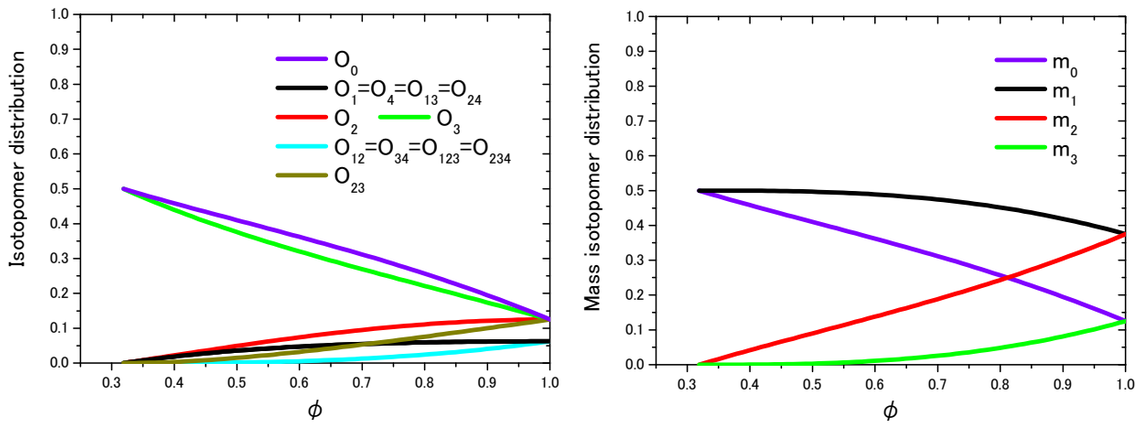

Fig. 9. Simulation result of (a) isotopomer and (b) mass isotopomer distributions of OAA with respect to ϕ for the case of using 100 % [1-^{13}C] glucose ($v_1 = 1.0$).

So far, we considered how the isotopomer distribution is expressed with respect to the flux. In practice, the fluxes must be found from the measured signals for the isotopomer distribution. Let these signals be obtained by either NMR or MS, and let these be $s_i (i = 1, 2, \cdots)$. Then the fluxes may be obtained by minimizing the following objective function:

$$J = (\hat{s} - s)^T \sum_S^{-1} (\hat{s} - s) \tag{12}$$

where s represents the measured signal vector containing s_i, $\hat{s}$ is its estimated vector, and $\sum_S$ is the variance-covariance matrix associated with the measured errors.

4. Dynamic behavior of isotopomer distribution

The metabolic flux analysis with ^{13}C-labeled substrate has been made based on the steady state condition. However, the sampling is usually made during instationary phase due to economical reason, and unsteady correction is made by assuming the 1st order washout behavior (van Winden et al., 2001). In many practical applications, this may be justified from

the viewpoint of the replacement of the broth by the labeled substrate. However, another dynamic behavior must be taken into account for the analysis of the TCA cycle, since the isotopomer distribution changes with respect to each turn of the TCA cycle. Although several analysis methods have been developed in the past for the special case of 100 % [2-^{13}C] acetate (Chance et al., 1983; Merle et al., 1996; Tran-Dinh et al., 1996a; Tran-Dinh et al., 1996b), here more general approach is considered.

Let Φ be the transition matrix which converts the isotopomer distribution at the i th turn to that at the $(i+1)$ th turn in the TCA cycle such that

$$x^{(i+1)} = \Phi \cdot x^{(i)} \tag{13}$$

where $x^{(i)}$ is the isotopomer vector at the i th turn of the TCA cycle. By considering the special cases of A_1=1, A_2=1, A_{12}=1, and A_0=1, respectively, and superimposing the results into one matrix, the general expression for Φ may be expressed as the matrix (Appendix A), letting $T \equiv v_{TCA}$, $G \equiv v_{Gly}$, $\beta \equiv 2^{-1}(T+G)$, and $\gamma \equiv T+2G$. Note that $T+2G=1$ holds. This expression for Φ may be useful in analyzing the transient behavior of the isotopomer distribution with respect to turn of the TCA cycle together with glyoxylate pathway. If we repeat the operation of Eq. (13), the following equation is obtained:

$$x^{(n)} = \Phi^n x^{(0)} \tag{14}$$

where $x^{(0)}$ is the isotopomer distribution vector before labeling experiment. This equation implies that the isotopomer distribution at the n th turn can be expressed once the initial state or at any known state was given, and this expression may be more useful than Eq. (13). Moreover, we can derive the same equations as Eq. (10) and (11) already derived in the steady state analysis if we set $n \to \infty$ (Appendix B). Thus, Eq. (14) can show not only steady state but also dynamic behavior of isotopomer. Appendix C shows the details of Φ^n.

As stated before, most of the flux analysis has been made based on the steady state assumption. However, this assumption must be carefully considered for the TCA cycle, since the ^{13}C-labeled isotopomer distribution changes for each turn of the TCA cycle. Figure 10a shows how the isotopomer distribution changes with respect to turn of the TCA cycle, where 100 % [2-^{13}C] acetate was used as a carbon source, and only TCA cycle was assumed to be active. Figure 10a indicates that O_2 and O_3 appear at the 1st turn, and O_{13} and O_{24} as well as O_{23} appear at the 2nd turn, but those reduced to zero as further cycling in the TCA cycle. On the other hand, O_{123} and O_{234} appear after the 3rd turn and converged to the steady state values. The converged values coincide with the values obtained by setting $z=0$ in the analytical expression (11). This result may be explained as follows: The C_2 position of AcCoA becomes C_4 position of CIT and αKG, and C_3 position of SUC, while C_5 position of CIT and αKG are never labeled if C_1 position of AcCoA is not labeled (Fig. 6). Randomization of carbons in SUC is made by allowing ^{13}C in the C_3 of SUC to be distributed equally to either C_2 or C_3 position of MAL in the first turn of the cycle. Thus at the end of the first turn of the cycle, O_2 and O_3 are produced with equal portions (Fig. 10a), which in the 2nd turn of the cycle generate C_{34} and C_{24} of CIT, C_{34} and C_{24} of αKG, and C_{23} and C_{13} of SUC. C_{23} of SUC only produces O_{23} since O_{23} is equivalent to O_{32}, while C_{13} of SUC produces equal amount of O_{24} and O_{13}. Condensation of these with C_2 of AcCoA (A_2) produces C_{234},C_{134}, and C_{246} of CIT, which eventually produce O_{123} and O_{234}.

Figure 10b shows the case where the glyoxylate pathway is active as well as TCA cycle. It indicates that at the first turn, O_2 and O_3 are generated, while O_{23},O_{123} and O_{234} appear as each turn is repeated, resulting in the eventual convergence to the steady state, where O_{23} newly appears as compared with the case of only TCA cycle. The converged values are the same as those computed using Eq. (11).

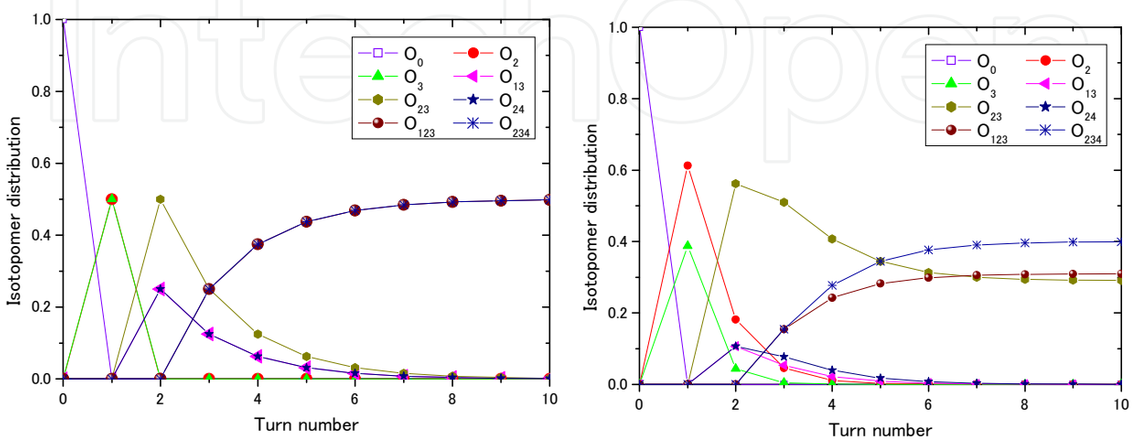

Fig. 10. Isotopomer distribution with respect to turn of the TCA cycle with glyoxylate pathway: Case of using the 100 % [2-^{13}C] acetate where (a) only TCA cycle is active, and (b) glyoxylate pathway as well as TCA cycle is active.

5. Metabolic regulation by global regulators in response to culture environment

The main goal of metabolic engineering is to improve the metabolic phenotype through genetic modifications (Bailey, 1991; Stephanopoulos & Vallino, 1991). Most of the past metabolic engineering approach has been considered to improve a particular biosynthetic capacity through engineering the target pathway. The resulting phenotypes are, however, often suboptimal and not satisfactory due to distant effects of genetic modifications or regulatory influences. It is, therefore, strongly desirable to take into account the metabolic regulation mechanism for metabolic engineering. Roughly speaking, metabolic regulation is made by recognition of culture environment (or cell's state) and the adjustment of the metabolism, where global regulators and/or sigma factors play important roles in regulating the metabolic pathway genes. Note that the high-throughput techniques for transcriptomics, proteomics, metabolomics, and fluxomics have the potential to disclose the metabolic regulation mechanism, but most of them provide a snapshot from one stage, and the methodology in interpreting different levels of information is not established yet (Vemuri & Aristidou, 2005). In order to put forward advanced fermentation toward biofuel production etc., it is quite important to understand the effect of culture environment on the metabolism based on gene level regulation, and modify the cell metabolism based on such information. In the followings, a brief explanation on the carbon catabolite regulation is given.

Global regulator	Metabolic pathway gene
Cra	+ : *aceBAK*, *acnA*, *cydB*, *fbp*, *icdA*, *pckA*, *pgk*, *ppsA* − : *acnB*, *adhE*, *eda*, *edd*, *pfkA*, *ptsHI*, *pykF*, *zwf*
Crp	+ : *acnAB*, *aceEF*, *acs*, *focA*, *fumA*, *fur*, *gltA*, *malT*, *manXYZ*, *mdh*, *mlc*, *pckA*, *pdhR*, *pflB*, *pgk*, *ptsG*, *sdhCDAB*, *sucABCD*, *ugpABCEQ* − : *cyaA*, *lpdA*, *rpoS*
ArcA/B	+ : *cydAB*, *focA*, *pflB* − : *aceBAK*, *aceEF*, *acnAB*, *cyoABCDE*, *fumAC*, *gltA*, *icdA*, *lpdA*, *mdh*, *nuoABCDEFGHIJKLMN*, *pdhR*, *sdhCDAB*, *sodA*, *sucABCD*
Fnr	+ : *acs*, *focA*, *frdABCD*, *pflB*, *yfiD* − : *acnAB*, *cyoABCDE*, *cydAB*, *fnr*, *fumA*, *icdA*, *ndh*, *nuoABCDEFGHIJKLMN*, *sdhCDAB*, *sucABCD*
IclR	− : *aceBAK*, *acs*
FadR	+ : *iclR*
SoxR/S	+ : *acnA*, *fumC*, *fur*, *sodA*, *zwf*
Mlc	− : *crr*, *manXYZ*, *malT*, *ptsG*, *ptsHI*
RpoS	+ : *acnA*, *acs*, *adhE*, *fumC*, *gadAB*, *osmC*, *poxB*, *talA*, *tktB* − : *ompF*
Fur	− : *entABCDE*, *sodA*
IclR	− : *aceBAK*, *acs*
PdhR	− : *aceEF*, *lpdA*
PhoB	+ : *phoABERU*, *pstSCAB*

Table 1. Effect of global regulators on the metabolic pathway gene expressions.

Among the culture environment, carbon sources are by far important for the cell from the point of view of energy generation (catabolism) and biosynthesis (anabolism). Catabolite

regulation is made when different carbohydrates are present in a medium, where glucose is preferentially consumed, and the uptake of other carbon sources is repressed. The center of the regulatory network for catabolite repression in *Escherichia coli* is the phosphoenol pyruvate (PEP): carbohydrate phosphotransferase systems (PTSs). These systems are involved in both transport and phosphorylation of carbohydrates. The PTS in *E. coli* consists of two common cytoplasmic proteins, EI (enzyme I) encoded by *ptsI* and HPr (histidine-phosphorylatable protein) encoded by *ptsH*, as well as carbohydrate-specific EII (enzyme II) complexes. The glucose-specific PTS in *E. coli* consists of the cytoplasmic protein $EIIA^{Glc}$ encoded by *crr* and the membrane-bound protein $EIICB^{Glc}$ encoded by *ptsG*, which transport and concomitantly phosphorylate glucose (Fig. 11). The phosphoryl groups are transferred from PEP via successive phosphorelay reactions in turn by EI, HPr, $EIIA^{Glc}$ and $EIICB^{Glc}$ to glucose. The cAMP-Crp complex and the repressor Mlc are involved in the regulation of *ptsG* gene and *pts* operon expressions. It has been demonstrated that unphosphorylated $EIICB^{Glc}$ can relieve the *ptsG* gene expression by sequestering Mlc from its binding sites through protein-protein interaction depending on the glucose concentration. In contrast to Mlc, which represses the expressions of *ptsG*, *ptsHI* and *crr* (Plumbridge, 1998), cAMP-Crp complex activates *ptsG* gene expression (De Reuse & Danchin, 1988). These two antagonistic regulatory mechanisms guarantee a precise adjustments of *ptsG* expression levels under various conditions (Bettenbrock et al., 2006). It should be noted that unphosphorylated $EIIA^{Glc}$ inhibits the uptake of other non-PTS carbohydrates by the so-called inducer exclusion (Aiba, 1995), while phosphorylated $EIIA^{Glc}$ ($EIIA^{Glc}$-P) activates adenylate cyclase (Cya), which generates cAMP from ATP and leads to an increase in the intracellular cAMP level (Park et al., 2006). In the absence of glucose, Mlc binds to the upstream of *ptsG* gene and prevents its transcription. If glucose is present in the medium, the amount of unphosphorylated $EIICB^{Glc}$ increases due to the phosphate transfer to glucose. In this situation, Mlc binds to $EIICB^{Glc}$, and thus it does not bind to the operator of *pts* genes (Bettenbrock et al., 2006; Tanaka et al., 2000; Lee et al., 2000). The overall catabolite regulation mechanism is briefly shown in Fig. 12 (Matsuoka & Shimizu, 2011). The catabolic regulation phenomenon has been modeled by several researchers (Bettenbrock et al., 2006; Kremling et al.; 2004; Kremling & Gilles, 2001).

In addition to cAMP-Crp, which acts depending on the level of glucose concentration, the catabolite repressor/activator protein (Cra) originally characterized as the fructose repressor (FruR) controls the carbon flow in *E. coli* (Moat et al., 2002; Saier, 1996; Saier & Ramseier, 1996). The carbon uptake and glycolysis genes such as *ptsHI*, *pfkA*, *pykF*, *zwf* and *edd-eda* are repressed, while gluconeogenic pathway genes such as *ppsA*, *fbp*, *pckA*, *icdA* and *aceA*, *B* are activated by Cra (Moat et al., 2002; Saier & Ramseier, 1996) (Table 1, Fig. 11). It has been known that the mutant defective in *cra* gene is unable to grow on gluconeogenic substrates such as pyruvate, acetate and lactate (Saier et al., 1996). Since gluconeogenic pathway genes are deactivated, and the glycolysis genes are activated by *cra* gene knockout, the glucose uptake rate may be enhanced, but it must be careful since *icdA*, *aceA*, *B*, and *cydB* genes are repressed, while *zwf* and *edd* gene expressions are activated and thus ED pathway is activated by *cra* gene knockout (Sarkar et al., 2008).

The effects of other culture environments than carbon source are given elsewhere (Matsuoka & Shimizu, 2011).

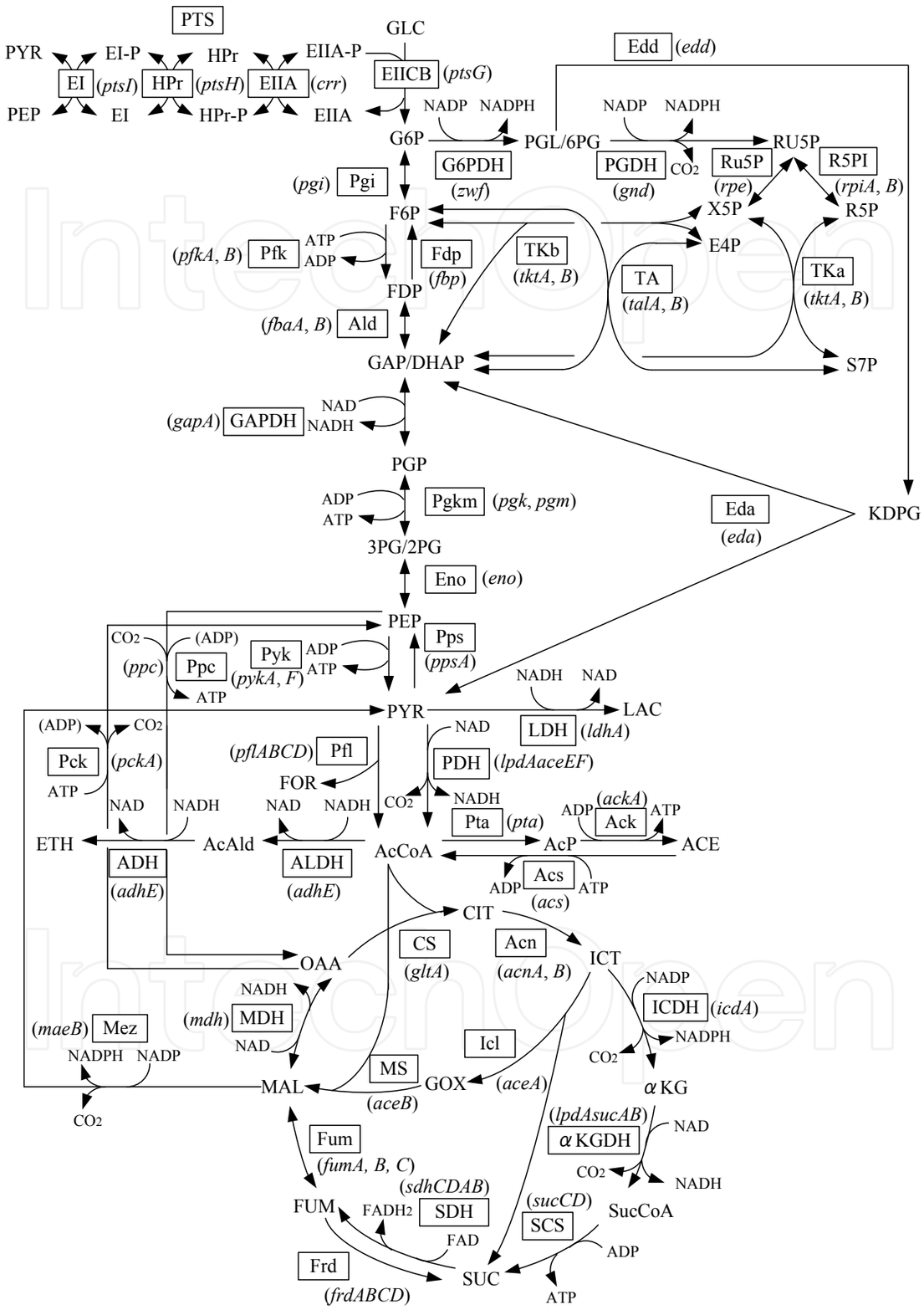

Fig. 11. Main metabolic pathways of *Escherichia coli*.

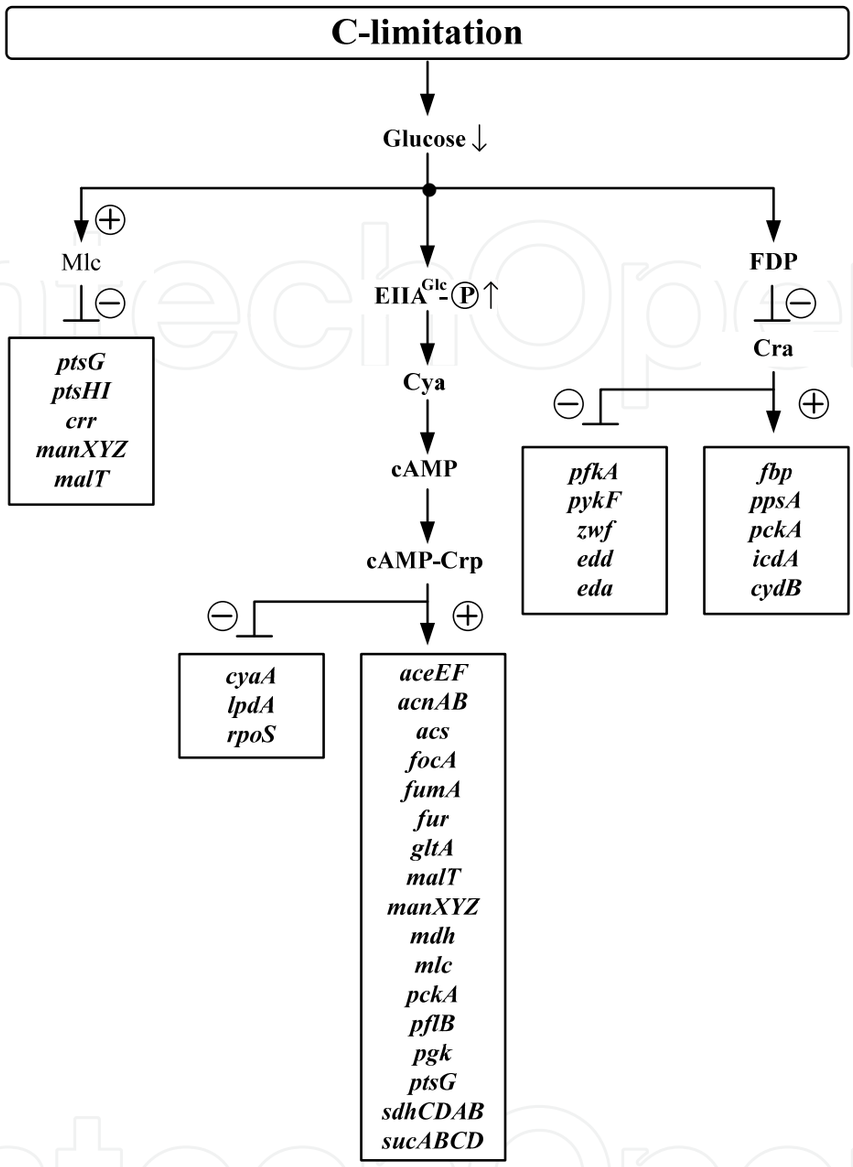

Fig. 12. Transcriptional regulation in response to carbon catabolite regulation.

6. Conclusion

^{13}C-Metabolic flux analysis is quite useful to understand the cell metabolism. In this chapter, analytical approach for ^{13}C-metabolic flux analysis is also explained to make the relationship between fluxes and isotopomer patterns to be transparent. Metabolic regulation occurs in response to culture environment. The global regulators sense such a change, and those regulate metabolic pathway genes. To predict cell metabolism in response to environmental change, the relationships between culture environment and global regulators and the relationships between global regulators and metabolic pathway genes have to be figured out. For this, it is desired to integrate different levels of information as well as ^{13}C-metabolic flux distribution.

7. Appendix A: The general expression for Φ.

$\Phi \equiv$

γA_0	$(T+G)A_0$	GA_0	GA_0	$(T+G)A_0$	GA_0	0	TA_0	0	0	GA_0	0	0	0	0	0
$(\beta+G)A_1$	$(2^{-1}T+G)A_1$ $+2^{-1}GA_0$	GA_1	$2^{-1}GA_1$ $+2^{-1}TA_0$	βA_1	GA_1	βA_0	$2^{-1}TA_1$ $+2^{-1}GA_0$	0	0	$2^{-1}GA_1$ $+2^{-1}TA_0$	0	0	βA_0	0	0
$(\beta+G)A_2$	$(2^{-1}T+G)A_2$	GA_2 $+\beta A_0$	$2^{-1}GA_2$	βA_2	GA_2 $+2^{-1}TA_0$	0	$2^{-1}TA_2$	$2^{-1}GA_0$	βA_0	$2^{-1}GA_2$	0	$2^{-1}TA_0$	0	$2^{-1}GA_0$	0
βA_2	$2^{-1}TA_2$	βA_0	$2^{-1}GA_2$ $+GA_0$	βA_2	$2^{-1}TA_0$	GA_0	$2^{-1}TA_2$	$(2^{-1}G+G)A_0$	βA_0	$2^{-1}GA_2$	GA_0	$2^{-1}TA_0$	0	$2^{-1}GA_0$	0
βA_1	$2^{-1}TA_1$ $+2^{-1}GA_0$	0	$2^{-1}GA_1$ $+2^{-1}TA_0$	βA_1 $+GA_0$	0	βA_0	$2^{-1}TA_1+$ $(2^{-1}G+G)A_0$	0	GA_0	$2^{-1}GA_1$ $+2^{-1}TA_0$	0	GA_0	βA_0	0	0
$(\beta+G)A_0$	$(2^{-1}T+G)A_{12}$	GA_{12}	$2^{-1}GA_{12}$	βA_{12}	$2^{-1}GA_0$ $+GA_{12}$	0	$2^{-1}TA_{12}$	$2^{-1}TA_0$	0	βA_{12}	βA_0	$2^{-1}GA_0$	0	$2^{-1}TA_0$	βA_0
0	$2^{-1}GA_2$	βA_1	GA_1 $+2^{-1}TA_2$	0	$2^{-1}TA_1$	GA_1 $+\beta A_2$	$2^{-1}GA_2$	$(2^{-1}G+G)A_1$	βA_1	$2^{-1}TA_2$	GA_1	$2^{-1}TA_1$	βA_2	$2^{-1}GA_1$	0
0	GA_1	0	TA_1	GA_1	0	$(\gamma+G)A_1$	$2GA_1$	0	GA_1	TA_1	0	GA_1	$(T+G)A_1$	0	0
0	0	$(\gamma+G)A_2$	GA_2	0	TA_2	GA_2	0	$2GA_2$	$(T+G)A_2$	0	GA_2	TA_2	0	GA_2	0
0	$2^{-1}GA_2$	βA_1	$2^{-1}TA_2$	GA_2	$2^{-1}TA_1$	βA_2	$(2^{-1}G+G)A_2$	$2^{-1}GA_1$	βA_1 $+GA_2$	$2^{-1}TA_2$	0	$2^{-1}TA_1$ $+GA_2$	βA_2	$2^{-1}GA_1$	0
βA_{12}	$2^{-1}TA_{12}$	0	$2^{-1}GA_{12}$	βA_{12}	$2^{-1}GA_0$	0	$2^{-1}TA_{12}$	$2^{-1}TA_0$	0	GA_0 $+\beta A_{12}$	βA_0	$2^{-1}GA_0$	GA_0	$(2^{-1}T+G)A_0$	$(\beta+G)A_0$
0	0	βA_{12}	GA_{12}	0	$2^{-1}GA_2$ $+2^{-1}TA_2$	GA_{12}	0	$2^{-1}TA_2+$ $(2^{-1}G+G)A_2$	βA_{12}	0	βA_2 $+GA_{12}$	$2^{-1}GA_2$ $+2^{-1}TA_2$	0	$2^{-1}TA_2$ $+2^{-1}GA_{12}$	βA_2
0	$2^{-1}GA_{12}$	0	$2^{-1}TA_{12}$	GA_{12}	$2^{-1}GA_1$	βA_{12}	$(2^{-1}G+G)A_{12}$	$2^{-1}TA_1$	GA_{12}	0	βA_1	$2^{-1}GA_1$ $+GA_{12}$	βA_{12}	$2^{-1}TA_1$	$(T+G)A_1$
0	$2^{-1}GA_{12}$	0	$2^{-1}TA_{12}$	0	$2^{-1}GA_1$	βA_{12}	$2^{-1}GA_{12}$	$2^{-1}TA_1$	0	GA_1	βA_1	$2^{-1}GA_1$	GA_1 $+\beta A_{12}$	$(2^{-1}T+G)A_1$	γA_1
0	0	βA_{12}	0	0	$2^{-1}GA_2$ $+2^{-1}TA_2$	0	0	$2^{-1}TA_2$ $+2^{-1}GA_{12}$	βA_{12}	GA_2	βA_2	$2^{-1}GA_2$ $+2^{-1}TA_2$	GA_2	$(2^{-1}T+G)A_2$ $+2^{-1}GA_{12}$	$(\beta+G)A_2$
0	0	0	0	0	GA_{12}	0	0	TA_{12}	0	GA_{12}	$(T+G)A_{12}$	GA_{12}	GA_{12}	$(T+G)A_{12}$	γA_{12}

8. Appendix B: Derivation of eq. (10) and (11) using Φ^n as $n \to \infty$

1. The case where $A_2 = 1$:

By inspection, if we assume n to be large enough, Φ^n can be reduced to

$$\Phi^n = \begin{bmatrix} 2G & G & G \\ 0.5T & 0.5(T+G) & 0.5T \\ 0.5T & 0.5(T+G) & 0.5T+G \end{bmatrix}^n \tag{B1}$$

where only the terms associated with O_{23}, O_{123} and O_{234} were left. Note that Φ can be diagonalized by multiplying the eigen matrix P and its inverse such that

$$P^{-1}\Phi P = \begin{bmatrix} \lambda_1 & 0 & 0 \\ 0 & \lambda_2 & 0 \\ 0 & 0 & \lambda_3 \end{bmatrix} \tag{B2}$$

where $\lambda_i \ (i = 1,2,3)$ are the distinct eigen values of Φ. Since we have the relationship

$$\left(P^{-1}\Phi P\right)^n = P^{-1}\Phi^n P \tag{B3}$$

Φ^n can be expressed as

$$\Phi^n = P\left(P^{-1}\Phi P\right)^n P^{-1} = P\begin{bmatrix} {\lambda_1}^n & 0 & 0 \\ 0 & {\lambda_2}^n & 0 \\ 0 & 0 & {\lambda_3}^n \end{bmatrix} P^{-1} \tag{B4}$$

Here $\lambda_i \ (i = 1,2,3)$ and P are obtained for Φ as follows:

$$\lambda_1 = G, \quad \lambda_2 = 2G + T, \quad \lambda_3 = \frac{G}{2}$$

$$P = \begin{bmatrix} & 1 & \\ 1 & & 0 \\ 0 & \dfrac{1}{T+G}\left\{\dfrac{T(2G+T)^2}{G(3G+2T)} - T\right\} & 1 \\ -1 & & -1 \\ & \dfrac{T(2G+T)}{G(3G+2T)} & \end{bmatrix} \tag{B5}$$

Then Φ^n could be calculated as

$$\Phi^n = \begin{bmatrix} G^n & (2G+T)^n & 0 \\ 0 & (2G+T)^n \dfrac{1}{T+G}\left\{\dfrac{T(2G+T)^2}{G(3G+2T)} - T\right\} & \left(\dfrac{G}{2}\right)^n \\ -G^n & (2G+T)^n \dfrac{T(2G+T)}{G(3G+2T)} & -\left(\dfrac{G}{2}\right)^n \end{bmatrix} \begin{bmatrix} \dfrac{T}{G+T} & -\dfrac{G}{G+T} & -\dfrac{G}{G+T} \\ \dfrac{G}{G+T} & \dfrac{G}{G+T} & \dfrac{G}{G+T} \\ -\dfrac{T}{3G+2T} & \dfrac{3G+T}{3G+2T} & -\dfrac{T}{3G+2T} \end{bmatrix}$$

$$= \begin{bmatrix} \dfrac{T}{G+T}G^n + \dfrac{G}{G+T}(2G+T)^n & \dfrac{G}{G+T}\left\{-G^n + (2G+T)^n\right\} & \dfrac{G}{G+T}\left\{-G^n + (2G+T)^n\right\} \\ \dfrac{T}{3G+2T}\left\{(2G+T)^n - \left(\dfrac{G}{2}\right)^n\right\} & \dfrac{T}{3G+2T}(2G+T)^n + \dfrac{3G+T}{3G+2T}\left(\dfrac{G}{2}\right)^n & \dfrac{T}{3G+2T}\left\{(2G+T)^n - \left(\dfrac{G}{2}\right)^n\right\} \\ -\dfrac{T}{G+T}G^n + \dfrac{T(2G+T)}{(3G+2T)(G+T)}(2G+T)^n + \dfrac{T}{3G+2T}\left(\dfrac{G}{2}\right)^n & \dfrac{G}{G+T}G^n + \dfrac{T(2G+T)}{(3G+2T)(G+T)}(2G+T)^n - \dfrac{3G+T}{3G+2T}\left(\dfrac{G}{2}\right)^n & \dfrac{G}{G+T}G^n + \dfrac{T(2G+T)}{(3G+2T)(G+T)}(2G+T)^n + \dfrac{T}{3G+2T}\left(\dfrac{G}{2}\right)^n \end{bmatrix} \tag{B6}$$

Noting that G is less than 1 and $2G + T = 1$, we have for $n \to \infty$

$$\Phi^\infty = \begin{bmatrix} \dfrac{G}{G+T} & \dfrac{G}{G+T} & \dfrac{G}{G+T} \\ \dfrac{T}{3G+2T} & \dfrac{T}{3G+2T} & \dfrac{T}{3G+2T} \\ \dfrac{T(2G+T)}{(3G+2T)(G+T)} & \dfrac{T(2G+T)}{(3G+2T)(G+T)} & \dfrac{T(2G+T)}{(3G+2T)(G+T)} \end{bmatrix} \tag{B7}$$

Then, we can derive the following relationships:

$$\begin{bmatrix} O_{23} \\ O_{123} \\ O_{234} \end{bmatrix} = \begin{bmatrix} \dfrac{G}{G+T} \\ \dfrac{T}{3G+2T} \\ \dfrac{T(2G+T)}{(3G+2T)(G+T)} \end{bmatrix} \tag{B8}$$

which is equivalent to Eq. (11) already derived previously for the steady state.

2. The case where $A_1 = 1$:

In the similar was as above, Φ^n is expressed for n to be large enough as follows:

$$\Phi^n = \begin{bmatrix} 2G & G & G \\ 0.5T & 0.5(T+G) & 0.5T \\ 0.5T & 0.5(T+G) & 0.5T+G \end{bmatrix}^n \tag{B9}$$

where only the terms associated with O_{14} , O_4 and O_1 are left. Then the steady state values could be obtained as follows:

$$\begin{bmatrix} O_{14} \\ O_4 \\ O_1 \end{bmatrix} = \begin{bmatrix} \dfrac{G}{G+T} \\ \dfrac{T}{3G+2T} \\ \dfrac{T(2G+T)}{(3G+2T)(G+T)} \end{bmatrix} \tag{B10}$$

where this equation is equivalent to Eq. (10) as previously derived for the steady state.

9. Appendix C: Isotopomer pattern of OAA at the n th turn of the TCA cycle together with glyoxylate pathway

Let us consider deriving the general case for $A_2 = 1$, where Φ can be reduced from 16×16 to 8×8 due to the limited appearance of the isotopomer as

$$\Phi = \begin{bmatrix} 0 & 0 & 0 & 0 & 0 & 0 & 0 & 0 \\ 2^{-1}(T+G)+G & G & 2^{-1}G & 0 & 0 & 0 & 0 & 0 \\ 2^{-1}(T+G) & 0 & 2^{-1}G & 0 & 0 & 0 & 0 & 0 \\ 0 & 0 & 2^{-1}T & 2^{-1}(T+G) & 0 & 0 & 0 & 0 \\ 0 & T+G & G & G & 2G & T+G & G & G \\ 0 & 0 & 2^{-1}T & 2^{-1}(T+G) & 0 & G & 0 & 0 \\ 0 & 0 & 0 & 0 & 2^{-1}T & 0 & 2^{-1}(T+G) & 2^{-1}T \\ 0 & 0 & 0 & 0 & 2^{-1}T & 0 & 2^{-1}(T+G) & 2^{-1}T+G \end{bmatrix} \tag{C1}$$

Let this matrix be subdivided into 4 submatrices as

$$\Phi = \begin{bmatrix} A(4\times 4) & 0(4\times 4) \\ B(4\times 4) & D(4\times 4) \end{bmatrix} \tag{C2}$$

Then it can be shown that the following equation holds

$$\Phi^n = \begin{bmatrix} A^n & 0 \\ B^n = \sum_{r=0}^{n-1} D^r B A^{n-r-1} & D^n \end{bmatrix} \tag{C3}$$

where A^n and D^n can be expressed as

$$A^n = \begin{bmatrix} 0 & 0 & 0 & 0 \\ -\frac{T+G}{G}2^{-n}G^n + \frac{T+2G}{G}G^n & G^n & -2^{-n}G^n + G^n & 0 \\ \frac{T+G}{G}2^{-n}G^n & 0 & 2^{-n}G^n & 0 \\ -\frac{T+G}{G}2^{-n}G^n + 2^{-n}(T+G)^n & 0 & -2^{-n}G^n + 2^{-n}(T+G)^n & 2^{-n}(T+G)^n \end{bmatrix} \tag{C4a}$$

$$D^n = \begin{bmatrix} \frac{T}{T+G}G^n + \frac{G}{T+G}(T+2G)^n & -\frac{T^2+TG+G}{T+G}G^n + T\left(nG^{n-1}+G^n\right) + \frac{G}{T+G}(T+2G)^n & -\frac{G}{T+G}G^n + \frac{G}{T+G}(T+2G)^n & -\frac{G}{T+G}G^n + \frac{G}{T+G}(T+2G)^n \\ 0 & G^n & 0 & 0 \\ -\frac{T}{2T+3G}2^{-n}G^n + \frac{T}{2T+3G}(T+2G)^n & -TG^{n-1} + \frac{2T(G+T)}{G(2T+3G)}2^{-n}G^n + \frac{T}{2T+3G}(T+2G)^n & \frac{T+3G}{2T+3G}2^{-n}G^n + \frac{T}{2T+3G}(T+2G)^n & -\frac{T}{2T+3G}2^{-n}G^n + \frac{T}{2T+3G}(T+2G)^n \\ -\frac{T}{T+G}G^n + \frac{T}{2T+3G}2^{-n}G^n + \frac{T(T+2G)}{(T+G)(2T+3G)}(T+2G)^n & \frac{T^2+TG+G}{T+G}G^n + T\left(-nG^{n-1} + \frac{-TG+T-G}{TG}G^n\right) \frac{2T(G+T)}{G(2T+3G)}2^{-n}G^n + \frac{T(T+2G)}{(T+G)(2T+3G)}(T+2G)^n & \frac{G}{T+G}G^n - \frac{T+3G}{2T+3G}2^{-n}G^n + \frac{T(T+2G)}{(T+G)(2T+3G)}(T+2G)^n & \frac{G}{T+G}G^n + \frac{T}{2T+3G}2^{-n}G^n + \frac{T(T+2G)}{(T+G)(2T+3G)}(T+2G)^n \end{bmatrix} \tag{C4b}$$

10. Acknowledgement

This research was supported in part by Strategic International Cooperative Program, Japan Science and Technology Agency (JST).

11. References

Aiba, H. (1995). The *lac* and *gal* operons today. In "Regulation of Gene expression in *Escherichia coli*.", In: Lin, E. C. C. & Lynch, A. S. (Ed.), Chap 9, pp. 182-200, Landes

Bailey, J. E. (1991). Toward a science of metabolic engineering. *Science*, vol.252, pp. 1668-1675

Bettenbrock, K.; Fischer, S.; Klemling, A.; Sauter, F. T.; Gilles, E. D. (2006) A quantitative approach to catabolite repression in *Escherichia coli*. *J. Biol. Chem.* Vol.281, pp. 2578-2584

Blank, L. M. & Sauer, U. (2004). TCA cycle activity in *Saccharomyces cerevisiae* is a function of the environmentally determined specific growth and glucose uptake rate. *Microbiology*, vol.150, pp. 1085-1093

Chance, E. M.; Seeholzer, S. H.; Kobayashi, K.; Williamson, J. R. (1983). Mathematical analysis of isotope labeling in the citric acid cycle with applications to ^{13}C NMR studies in perfused rat hearts. *J. Biol. Chem.*, vol.258, No.22, pp. 13785-13794

Edwards, J. S. & Palsson, B. O. (2000). The *Escherichia coli* MG1655 in silico metabolic genotype: its definition, characteristics, and capabilities. *PNAS*, vol.97, pp. 5528-5533

Fischer, E. & Sauer, U. (2003). Metabolic flux profiling of *Escherichia coli* mutants in central carbon metabolism by GC-MS. *Eur. J. Biochem.*, vol.270, pp. 880-891

Fuhrer, T.; Fischer, E.; Sauer, U. (2005). Experimental identification and quantification of glucose metabolism in seven bacterial species. *J. Bacteriol.*, vol.187, pp. 1581-1590

Hellerstein, M. K. (2004). New stable isotope-mass spectrometric techniques for measuring fluxes through intact metabolic pathways in mammarian systems: introduction of moving pictures into functional genomics and biochemical phenotyping. *Metab. Eng.*, vol.6, pp. 85-100

Hua, Q.; Yang, C.; Baba, T.; Mori, H.; Shimizu, K. (2003). Responses of the central carbon metabolism in *Escherichia coli* to phosphoglucose isomerase and glucose-6-phosphate dehydrogenase knockouts. *J. Bacteriol.*, vol.185, pp. 7053-7067

Kelleher, J. K. (2004). Probing metabolic pathways with isotopic tracers: insights from mammarian metabolic pathways. *Metab. Eng.*, vol.6, pp. 1-5

Kremling, A.; Fischer, S.; Sauter, T.; Bettenbrock, K.; Gilles, E. D. (2004). Time hierarchies is the *Escherichia coli* carbohydrate uptake and metabolism. *BioSystems*, vol.73, pp. 57-71

Kremling, A. & Gilles, E. D. (2001). The organization of metabolic reaction networks. II. Signal processing in hierarchical structured functional units. *Metab. Eng.*, vol. 3, pp. 138-150

Lee, S. J.; Boos, W.; Bouché, J. P.; Plumbridge, J. (2000). Signal transduction between a membrane-bound transporter, PtsG, and a soluble transcription factor, Mlc, of *Escherichia coli*. *EMBO J.*, vol.19, pp. 5353-5361

Marx, A.; Graaf, A. A.; Wiechert, W.; Eggeling, L.; Sahm, H. (1996). Determination of the fluxes in the central metabolism of *Corynebacterium glutamicum* by nuclear magnetic resonance spectroscopy combined with metabolite balancing. *Biotechnol. Bioeng.*, vol.49, pp. 111-129

Matsuoka, Y. & Shimizu, K. (2010a). Current status of ^{13}C-metabolic flux analysis and future perspectives. *Process Biochemistry*, vol.45, pp. 1873-1881

Matsuoka, Y. & Shimizu, K. (2010b). The relationships between the metabolic fluxes and ^{13}C-labeled isotopomer distribution for the flux analysis of the main metabolic pathways. *Biochem. Eng. J.*, vol. 49, pp. 326-336

Matsuoka, Y. & Shimizu, K. (2011) Metabolic regulation in *Escherichia coli* in response to culture environments via global regulators. *Biotechnol. J.*, DOI: 10.1002/biot.201000447

McCabe, B. J.& Previs, S. F. (2004). Using isotope tracers to study metabolism: Application in mouse models. *Metabolic Eng.*, vol.6, pp. 25-35

Merle, M.; Martin, M.; Villegier, A.; Canioni, P. (1996). Mathematical modelling of the citric acid cycle for the analysis of glutamate isotopomers from cerebellar astrocytes incubated with [1-^{13}C] glucose. *Eur. J. Biochem.*, vol.239, pp. 742-751

Moat, A. G.; Foster, J. W.; Spector, M. P. (2002). (Ed.), In Microbial Physiology, John Wiley & Sons

Park, Y. H.; Lee, B. R.; Seok, Y. J.; Peterkofsky, A. (2006). *In vitro* reconstruction of catabolite repression in *Escherichia coli*. *J. Biol. Chem.*, vol.281, pp. 6448-6454

Plumbridge, J. (1998). Expression of *ptsG*, the gene for the major glucose PTS transporter in *Escherichia coli*, is repressed by Mlc and induced by growth on glucose. *Mol. Microbiol.*, vol.29, pp. 1053-1063

Price, N. D; Papin, J. A.; Schilling, C. H.; Palsson, B. O. (2003). Genome-scale microbial *in silico* models: the constraints-based approach. *Trends Biotechnol.*, vol.21, pp. 162-169

Raghevendran, V.; Gombert, A. K.; Christensen, B.; Kotter, P.; Nielsen, J. (2004). Phenotypic characterization of glucose repression mutants of *Saccharomyces cerevisiae* using experiments with 13C-labelled glucose. *Yeast*, vol. 21, pp. 769-779

De Reuse, H.; Danchin, A. (1988). The *ptsH*, *ptsI* and *crr* genes of the *Escherichia coli* phosphoenolpyruvate-dependent phosphotransferase system: a complex operon with several modes of transcription. *J. Bacteriol.*, vol.179, pp. 3827-3837

Rothman, D. L.; Behar, K. L.; Hyder, F.; Shulman, R. G.. (2003). *In vivo* NMR studies on the glutamate neurotransmitter flux and neuroenergetics: implications for brain function. *Ann. Rev. Physiol.*, vol.65, pp. 401-427

Saier, M. H., Jr. (1996). Cyclic AMP-independent catabolite repression in bacteria. *FEMS Microbiol. Lett.*, vol.138, pp. 97-103

Saier, M. H., Jr. & Ramseier, T. M. (1996). The catabolite repressor/activator (Cra) protein of enteric bacteria. *J. Bacteriol.*, vol.178, pp. 3411-3417

Saier, M. H., Jr.; Ramseier, T. M.; Reizer, J. (1996). Regulation of carbon utilization, in: Neidhardt, F. C., Curtiss III, R., Ingraham, J. L., Lin, E. C. C., Low, K. B., Magasanik, B., Reznikoff, W. S., Riley, M., Schaechter, M., and Umbarger, H. E. (Ed.), *Escherichia coli* and *Salmonella*: cellular and molecular biology, 2nd ed., vol. 1. ASM Press, pp.1325-1343, Washington, D.C.

Sarkar, D.; Siddiquee, K. A.; Araúzo-Bravo, M. J.; Oba, T.; Shimizu, K. (2008). Effect of *cra* gene knockout together with *edd* and *iclR* genes knockout on the metabolism in *Escherichia coli*. *Arch. Microbiol.*, vol. 190, pp. 559-571

Sarkar, D.; Yabusaki, M.; Hasebe, Y.; Ho, P. Y.; Kohmoto, S.; Kaga, T; Shimizu, K. (2010). Fermentation and metabolic characteristics of *Gluconacetobacter oboediens* for different carbon sources. *Appl. Microbiol. Biotechnol.*, vol. 87, pp. 127-136

Sauer, U. (2004). High-throughput phenomics: experimental methods for mapping fluxomes. *Curr. Opin. Biotechnol.*, vol.15, pp. 58-63

Sauer, U. (2006). Metabolic networks in motion: 13C-based flux analysis. *Molecular systems biology*, 2:62.

Sauer, U.; Hatzimanikatis, V.; Bailey, J. E.; Hochuli, M.; Szyperski, T.; Wüthrich, K. (1997). Metabolic fluxes in riboflavin-producing *Bacillus subtilis*. *Nat. Biotechnol.*, vol.15, pp. 448-452

Sauer, U.; Lasko, D. R.; Fiaux, J.; Hochuli, M.; Glaser, R.; Szyperski, T.; Wüthrich, K.; Bailey, J. E. (1999). Metabolic flux ratio analysis of genetic and environmental modulations of *Escherichia coli* central carbon metabolism. *J. Bacteriol.*, vol.181, pp. 6679-6688

Schilling, C. H. & Palsson, B. O. (1998). The underlying pathway structure of biochemical reaction netwoks. *PNAS*, vol.95, pp. 4193-4198

Schmidt, K.; Nielsen, J.; Villadsen, J. (1999). Quantitative analysis of metabolic fluxes in *Escherichia coli*, using two-dimensional NMR spectroscopy and complete isotopomer models. *J. Biotechnol.*, vol.71, pp. 175-190

Schuetz, R.; Kuepfer, L.; Sauer, U. (2007). Systematic evaluation of objective functions for predicting intracellular fluxes in *Escherichia coli*. *Mol. Syst. Biol.*, vol.3, pp. 1-14

Schwender, J.; Goffman, F.; Ohlrogge, J.; Shachar-Hill, Y. (2004). Rubisco without the Calvin cycle improves the carbon efficiency of developing green seeds. *Nature*, vol.432, pp. 779-782

Selivanov, V. A.; Meshalkina, L. E.; Solovjeva, O. N.; Kuche, P. W.; Ramos-Montoya, A.; Kochetov, G. A.; Lee, P. W. N.; Cascante, M. (2005). Rapid simulation and analysis of isotopomer distributions using constraints based on enzyme mechanisms: an example from HT29 cancer cells. *Bioinformatics*, vol.21, pp. 3558-3564

Selivanov, V. A.; Sukhomlin, T.; Centelles, J. J.; Lee, P. W. N.; Cascante, M. (2006). Integration of enzyme kinetic models and isotopomer distribution analysis for studies of in situ cell operation. *BMC Neuroscience*, vol.7, pp. 1-15

Sherry, A. D.; Jeffrey, F. M.; Malloy, C. R. (2004). Analytical solutions for 13C isotopomer analysis of complex metabolic conditions: substrate oxidation, multiple pyruvate cycles, and gluconeogenesis. *Metab. Eng.*, vol.6, pp. 12-24

Sidorenko, Y.; Wahl, A.; Dauner, M.; Genzel, Y.; Reichl, U. (2008). Comparison of metabolic flux distributions for MDCK cell growth in glutamine- and pyruvate-containing media. *Biotech. Prog.*, vol.24, pp. 311-320

Stephanopoulos, G. N. (1999). Metabolic fluxes and metabolic engineering. *Metab. Eng.*, vol.1, pp. 1-11

Stephanopoulos, G. N.; Aristidou, A. A.; Nielsen, J. (1998). Metabolic Engineering, Acad. Press, SanDiego

Stephanopoulos, G.. & Vallino, J. J. (1991). Network rigidity and metabolic engineering in metabolite overproduction. *Science*, vol. 252, pp. 1675-1681

Szyperski, T. (1995). Biosynthetically directed fractional ^{13}C-labeling of proteinogenic amino acids —An efficient analytical tool to investigate intermediary metabolism. *Eur. J. Biochem.*, vol.232, pp. 433-448

Szyperski, T.; Glaser, R. W.; Hochuli, M.; Fiaux, J. (1999). Bioreaction network topology and metabolic flux ratio analysis by biosynthetic fractional ^{13}C labeling and two-dimensional NMR spectroscopy. *Metab. Eng.*, vol.1, pp. 189-197

Tanaka, Y.; Kimata, K.; Aiba, H. (2000). A novel regulatory role of glucose transporter of *Escherichia coli*: membrane sequestration of a global repressor Mlc. *EMBO J.*, vol.19, pp. 5344-5352

Tran-Dinh, S.; Beganton, F.; Nguyen, T.; Bouet, F.; Herve, M. (1996b). Mathematical model for evaluating the Krebs cycle flux with non-constant glutamate-pool size by ^{13}C-NMR spectroscopy. Evidence for the existence of two types of Krebs cycles in cells. *Eur. J. Biochem.*, vol.242, pp. 220-227

Tran-Dinh, S.; Bouet, F.; Huynh, Q.; Herve, M. (1996a). Mathematical models for determining metabolic fluxes through the citric acid and the glyoxylate cycles in *Saccharomyces cerevisiae* by ^{13}C-NMR spectroscopy. *Eur. J. Biochem.*, vol.242, pp. 770-778

Vemuri, G. N. & Aristidou, A. A. (2005). Metabolic engineering in the –omics era: elucidating and modulating regulatory networks. *Microbiol. Mol. Biol. Rev.*, vol.69, pp. 197-216

Wiechert, W. & de Graaf A. A. (1997). Bidirectional reaction steps in metabolic networks: I. Modeling and simulation of carbon isotope labeling experiments. *Biotech. Bioeng.*, vol.55, pp. 101-117

van Winden, W.; Schipper, D.; Verheijen, P.; Heijen, J. (2001). Innovations in generation and analysis of 2D [^{13}C, ^{1}H] COSY NMR spectra for metabolic flux analysis purpose. *Metab. Eng.*, vol.3, pp. 322-343

Wittmann, C. (2007). Fluxome analysis using GC-MS. *Microbiol. Cell Factories*, vol.6, pp. 1-17

Yang, C.; Hua, Q.; Shimizu, K. (2002). Metabolic flux analysis in Synechocystis using isotope distribution from ^{13}C-labeled glucose. *Metab. Eng.*, vol.4, pp. 202-216

Yang, C.; Hua, Q.; Shimizu, K. (2002). Integration of the information from gene expression and metabolic fluxes for the analysis of the regulatory mechanisms in *Synechocystis*. *Appl. Microbiol. Biotech.*, vol.58, pp. 813-822

Zhao, J.; Baba, T.; Mori, H.; Shimizu, K. (2004). Global metabolic response of *Escherichia coli* to *gnd* or *zwf* gene-knockout, based on ^{13}C-labeling experiments and the measurement of enzyme activities. *Appl. Microbiol. Biotech.*, vol.64, pp. 91-98

Zhu, J. & Shimizu, K. (2004). The effect of *pfl* genes knockout on the metabolism for optically pure D-lactate production by *Escherichia coli*. *Appl. Microbiol. Biotechnol.*, vol.64, pp. 367-375

Zhu, J. & Shimizu, K. (2005). Effect of a single-gene knockout on the metabolic regulation in *E. coli* for D-lactate production under microaerobic condition. *Metab. Eng.*, vol.7, pp. 104-115

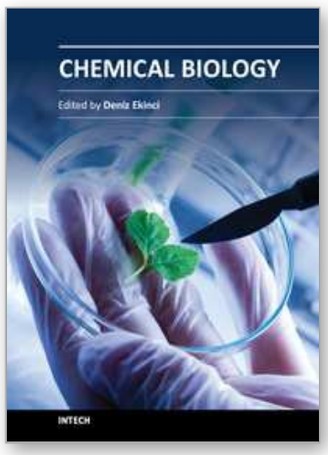

Chemical Biology

Edited by Prof. Deniz Ekinci

ISBN 978-953-51-0049-2
Hard cover, 444 pages
Publisher InTech
Published online 17, February, 2012
Published in print edition February, 2012

Chemical biology utilizes chemical principles to modulate systems to either investigate the underlying biology or create new function. Over recent years, chemical biology has received particular attention of many scientists in the life sciences from botany to medicine. This book contains an overview focusing on the research area of protein purification, enzymology, vitamins, antioxidants, biotransformation, gene delivery, signaling, regulation and organization. Particular emphasis is devoted to both theoretical and experimental aspects. The textbook is written by international scientists with expertise in synthetic chemistry, protein biochemistry, enzymology, molecular biology, drug discovery and genetics many of which are active chemical, biochemical and biomedical research. The textbook is expected to enhance the knowledge of scientists in the complexities of chemical and biological approaches and stimulate both professionals and students to dedicate part of their future research in understanding relevant mechanisms and applications of chemical biology.

INTECH
open science | open minds

InTech Europe
University Campus STeP Ri
Slavka Krautzeka 83/A
51000 Rijeka, Croatia
Phone: +385 (51) 770 447
Fax: +385 (51) 686 166
www.intechopen.com

InTech China
Unit 405, Office Block, Hotel Equatorial Shanghai
No.65, Yan An Road (West), Shanghai, 200040, China
中国上海市延安西路65号上海国际贵都大饭店办公楼405单元
Phone: +86-21-62489820
Fax: +86-21-62489821

IntechOpen